algorithms

MDPI

Article

Utilizing the Particle Swarm Optimization Algorithm for Determining Control Parameters for Civil Structures Subject to Seismic Excitation

Courtney A. Peckens *, Andrea Alsgaard, Camille Fogg, Mary C. Ngoma and Clara Voskuil

Department of Engineering, Hope College, 27 Graves Place, Holland, MI 49423, USA; andie.alsgaard@gmail.com (A.A.); camillemonet7@gmail.com (C.F.); mary.ngoma@hope.edu (M.C.N.); clara.voskuil@hope.edu (C.V.)

* Correspondence: peckens@hope.edu; Tel.: +1-616-395-7021

Abstract: Structural control of civil infrastructure in response to large external loads, such as earthquakes or wind, is not widely employed due to challenges regarding information exchange and the inherent latencies in the system due to complex computations related to the control algorithm. This study employs front-end signal processing at the sensing node to alleviate computations at the control node and results in a simplistic sum of weighted inputs to determine a control force. The control law simplifies to $U = WP$, where U is the control force, W is a pre-determined weight matrix, and P is a deconstructed representation of the response of the structure to the applied excitation. Determining the optimal weight matrix for this calculation is non-trivial and this study uses the particle swarm optimization (PSO) algorithm with a modified homing feature to converge on a possible solution. To further streamline the control algorithm, various pruning techniques are combined with the PSO algorithm in order to optimize the number of entries in the weight matrix. These optimization techniques are applied in simulation to a five-story structure and the success of the resulting control parameters are quantified based on their ability to minimize the information exchange while maintaining control effectiveness. It is found that a magnitude-based pruning method, when paired with the PSO algorithm, is able to offer the most effective control for a structure subject to seismic base excitation.

Keywords: structural control; wireless sensors; particle swarm optimization; pruning

Citation: Peckens, C.A.; Alsgaard, A.; Fogg, C.; Ngoma, M.C.; Voskuil, C. Utilizing the Particle Swarm Optimization Algorithm for Determining Control Parameters for Civil Structures Subject to Seismic Excitation. *Algorithms* **2021**, *14*, 292. https://doi.org/10.3390/a14100292

Academic Editors: Xiao-Zhi Gao and Allouani Fouad

Received: 9 September 2021
Accepted: 5 October 2021
Published: 8 October 2021

1. Introduction

Civil infrastructure (e.g., bridges and buildings) is highly susceptible to damage when subject to large external load events, such as high winds or earthquakes. Active structural control is an attractive method for mitigating this undesired response in such structures as it applies counterbalancing forces using an actuating device [1]. Such systems require a high level of integration between sensors that measure the response of the structure (e.g., displacement, velocity, and acceleration), computational nodes that determine appropriate reactions, and actuators that apply these counteracting forces. While active control methods have been successfully implemented in civil infrastructure [2–4], the successful coordination of communication between nodes and the necessary rapid response at the computational node have proved to be challenging. In order to increase the flexibility of these systems, the research community has turned to using low-power computing nodes equipped with wireless communication capabilities for the three control tasks (i.e., sensing, computing, and actuating) [5–7].

Wireless sensing units (WSUs) are individualized data acquisition units that are typically comprised of several key components. In particular, they contain an on-board microcontroller which enables localized data processing and allows them to serve as the controller in the actuation network. They are equipped with analog-to-digital converters

that allow them to seamlessly interface with transducers and serve as a sensing node. They also contain digital-to-analog converters or pulse width modulation output, such that they can interface with actuators and act as the actuation node. Finally, their on-board wireless transceiver enables peer-to-peer communication to allow for information exchange across the network. While the wireless technology does streamline communication, it also creates additional challenges such as a higher probability of data loss, which can degrade the control effectiveness [7]. Furthermore, while the on-board microcontroller does increase the flexibility of the unit, complex control algorithms can inhibit the real-time control capabilities of the system due to the limited computational capacity of the unit.

This work focuses on addressing these challenges by using a simplistic weighted-sum control algorithm that is designed to shift the computational demand to the sensing nodes and enable real-time control, while also minimizing communication. To achieve this, a method for determining weights in the control algorithm is needed and it is proposed to pair the particle swarm optimization (PSO) method with pruning mechanisms to further streamline the control law. This paper is structured as follows: (1) in Section 2, a literature review is presented; (2) in Section 3, the particle swarm optimization algorithm and the weighted-sum control algorithm are introduced; (3) in Section 4, the benchmark structure is defined and the algorithm is applied; (4) in Section 5, a pruning technique with PSO retraining is applied; and (5) Section 6 concludes the paper with a discussion.

2. Literature Review

Numerous researchers have explored various control architectures for civil structures that can be embedded on low-power computing cores, with a specific attempt to address the communication constraints of WSUs. In particular, these often focus on distributing traditional optimal control algorithms across a network of computing nodes and typically depend on using complex state estimators. In [8], a partially decentralized linear quadratic regulator (LQR) control scheme that leverages a Kalman filter to estimate unknown system states was validated on a full scale structure. In [9], a sparse representation of the LQR was proposed, which requires less information for decision-making than a traditional centralized approach, thereby reducing information flow requirements. In [10], the authors proposed a distributed H_∞ algorithm for civil infrastructure, and in [11], the authors explored distributing the H_∞ algorithm across multiple communication subnets of wireless sensing nodes. While these studies demonstrate the successful use of low-power computing cores in control architectures, they also highlight several challenges associated with this technology. Such challenges include increased computational requirements at the already resource-constrained sensing node and decision-making based on reduced information, resulting in some degradation in the control effectiveness.

The proportional-integrator-derivative (PID) controller has also been considered in numerous studies due to its ease of implementation, which often makes it less computationally expensive. Developing the control parameters for the PID controller for seismic control of structures is challenging because the off-diagonal terms in the damping and stiffness matrices of the structure cause cross-coupling in the system. As a result, traditional empirical methods for deriving the control parameters, such as the Ziegler–Nichols method, are often ineffective. However, numerous researchers have focused on using metaheuristic algorithms, such as the particle swarm optimization [12–15] and the genetic algorithm [16–19], to determine the PID control parameters for a variety of applications and these can be extended to the control of civil structures. In [20], the PSO algorithm was used to derive the PID coefficients for mitigating the effect of high-impact loads on a highway bridge, modeled as a single input–single output system. In [21], a genetic algorithm was used to derive the control parameters for a PID controller for a single active tuned mass damper (ATMD) and was applied to numerically control an 11-story building. In [22], the authors combined the LQR control scheme with a PID controller using the cuckoo search algorithm and validated the controller in simulation on a seismically excited 10-story structure equipped with a single ATMD. In [23], a new evolutionary algorithm was proposed to

derive the variables for a combined PID-LQR controller, which is numerically validated on a four-degree-of-freedom building that was equipped with an active control device on each floor. While all of these studies demonstrate the effectiveness of these methods, all but one is limited to a single output mechanism and they did not discuss communication considerations that would be encountered in real-world implementations of the structure. In [24], the authors did account for these communication and computational constraints by including time delays, while also exploring various metaheuristic methods for developing PID control parameters, and found that such delays could severely inhibit the control effectiveness.

In this study, the authors seek to address the real-world challenges experienced when implementing seismic control of structures through consideration of communication constraints and the computational complexity of the control algorithm. In particular, we propose to use a novel sensing node that is capable of real-time spectral decomposition to alleviate computations at the controlling node. This node also deviates from traditional Nyquist data acquisition rates and, as a result, minimizes the amount of transmitted data across the network. By leveraging the front-end signal processing of the sensing node, the control algorithm is reduced to a simplistic weighted sum of inputs that is easily executed. Other metaheuristic methods were previously explored in [25] and the PSO method was proven to be an effective method for determining parameters in this weighted-sum algorithm. This study continues to use the PSO method and focuses on further streamlining the weighted-control parameters to enhance the real-time control capabilities.

3. Adaptation of Particle Swarm Optimization and the Proposed Weighted Control Algorithm

Particle swarm optimization (PSO) is an iterative, population-based learning technique that is derived from the idea of swarm intelligence [26]. In PSO, a number of particles are dispersed randomly in a search space and each particle location is evaluated according to a specified fitness function. With each iteration of the algorithm, every particle moves to a new location in the search space based on its own history as well as on the behavior of other nearby particles. The overarching goal of the particle is to move closer to the optimum of the fitness function. To achieve this, each particle in the swarm tracks three vectors: $\boldsymbol{x}$, which is the current position of the particle, $\boldsymbol{v}$, which is its current velocity, and $\boldsymbol{x_b}$, which is the previous best position of the particle. Each particle also interacts with neighboring particles and stores the best position found from all neighbors, g, in order to leverage the benefits of the swarm.

Each particle updates its three vectors every iteration through the equations:

$$v_i(k+1) = \lambda v_i(k) + \rho_1\gamma_1(x_{b,i}(k) - x_i(k)) + \rho_2\gamma_2(g(k) - x_i(k)), \quad (1)$$

$$x_i(k+1) = x_i(k) + v_i(k+1), \quad (2)$$

and

$$\lambda = \lambda \times \tau, \quad (3)$$

where i is the particle number, k is the iteration number, ρ_1 and ρ_2 are random numbers between 0 and 1, and γ_1 and γ_2 are the acceleration coefficients which are both assigned to be 2 as recommended in [26]. Equation (3) also includes an inertia weight, λ, which affects the convergence and plays a role in balancing the desire of the particle to search locally versus globally [27]. An inertia damping constant, τ, is used to gradually modify this balance. λ is initially assigned to be 1 and is decreased using τ equal to 0.99 [28], which results in a global search that gradually becomes more localized. At the end of each iteration, each position of the particle is evaluated according to a fitness function and the best position is updated if applicable.

As will be discussed, the search space in this particular application has high dimensionality ($x \in \mathbb{R}^{275x1}$) and each element in the vector can assume a large range of values, from -1E8 to 1E8. As a result, it is easy for a particle to diverge from a localized optimal

solution, resulting in an extremely large cost function. To alleviate this challenge, the algorithm was modified to include a homing mechanism for the particle. If the fitness function of the particle significantly exceeds the fitness found from the best position of all of the neighbors, the particle returns to its previously identified local best position. The particle also resets its velocity to zero to prevent it from quickly diverging again. This modified PSO algorithm is termed PSO-H. The algorithm is depicted in the block diagram shown in Figure 1.

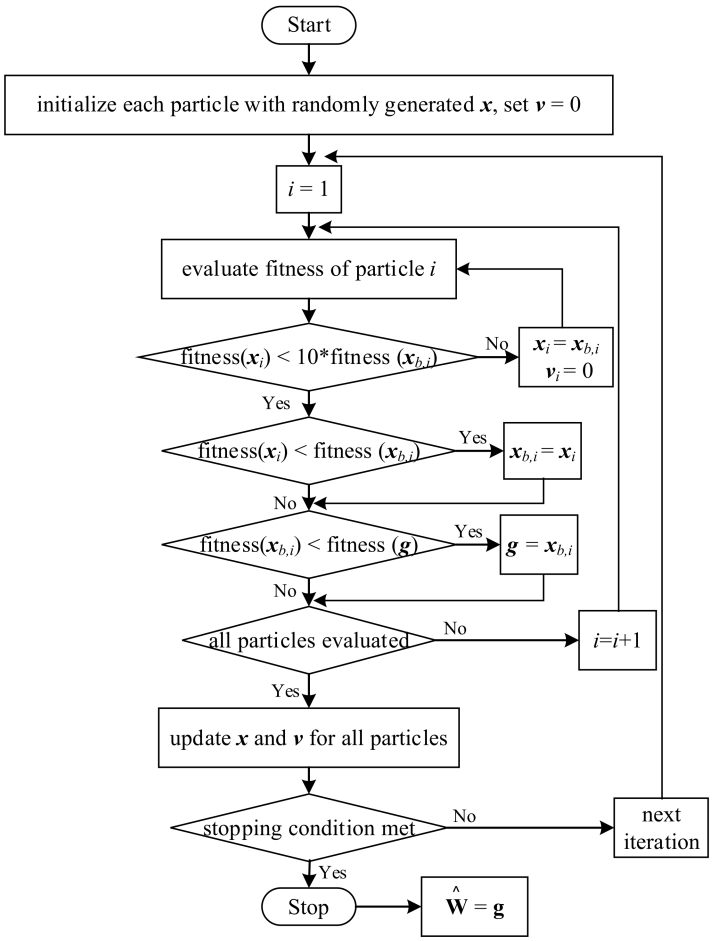

Figure 1. Flow chart for PSO-H algorithm.

The PSO-H algorithm is used to optimize the necessary control parameters for executing a control algorithm that was originally proposed in [25]. At the core of this algorithm is a novel sensing paradigm that is based on the mechanisms employed by the mammalian cochlea, first implemented by Peckens and Lynch for structural monitoring purposes [29,30]. In this paradigm, the response of the structure is decomposed into its frequency components in real-time using a series of overlapping bandpass filters. As discussed in [11,12], this bank of bandpass filters is optimized to fit the input signal by modifying the number of filters in the bank as well as their center frequency increments and passband frequency. The ability of this filter bank to decompose a signal into frequency components is attractive for the purposes of control, as it allows for instantaneous feature extraction, resulting in minimal signal processing at the actuation node.

The frequency selectivity of the jth filter is defined by the second-order transfer function for a bandpass filter [31], expressed as

$$H_j(s) = H_0 \frac{\omega_j}{Q_{0,j}} s \left(s^2 + \frac{\omega_j}{Q_{0,j}} s + {\omega_j}^2 \right)^{-1}, \quad (4)$$

where H_0 is set to 1.0 to ensure a unit gain in the filter and $Q_{0,j}$ is related to the frequency selectivity of the filter, defined as $(2\xi_j)^{-1}$, such that ξ_j is the damping ratio of the filter and ω_j is the center frequency of the filter (rad/s). By making these substitutions for H_0 and $Q_{0,j}$ in Equation (4), the impulse response of that filter is determined through the inverse Laplace transform, yielding

$$h_j(t) = -2\xi_j\omega_j\left(\sqrt{1-\xi_j{}^2}\right)^{-1} e^{\xi_j\omega_j t}\sin\left(\omega_j\sqrt{1-\xi_j{}^2}t-\theta\right), \tag{5}$$

with

$$\theta(t) = \tan^{-1}\left(\omega_j\sqrt{1-\xi_j{}^2}t-\theta\right). \tag{6}$$

The convolution integral can be used with the input signal, $y(t)$, and the impulse response of that filter, $h_j(t)$, to obtain the continuous time output of each jth bandpass filter, $z_j(t)$,

$$z_j(t) = \int_0^t y(\tau)h_j(t-\tau)d\tau. \tag{7}$$

Decomposing the signal into numerous components via bandpass filters increases the amount of information to manage, which is actually counterproductive to the goal of streamlining the control algorithm and communication. As such, the filtered signals, $z_j(t)$, are passed through a simple peak-picking algorithm and only these peak values are transmitted to the controller in an asynchronous sampling scheme. This allows for the control law to become a weighted sum of these peaks, expressed as

$$u(t_c) = \hat{W}P(k_p)\ , \tag{8}$$

where $u(t_c)$ is the calculated control value at control time increment t_c, $\hat{W}\ \epsilon\ \mathbb{R}^{1xn}$ is a control weighting vector, and $P(k_p)\ \epsilon\ \mathbb{R}^{nx1}$ is the vector of the detected peak values for all filters, given that n is the total number of filters. This complete process is depicted in Figure 2. For simplicity, the architecture shown in Figure 2 is a single input–single output system but it could easily be extended to a multiple input–multiple output system.

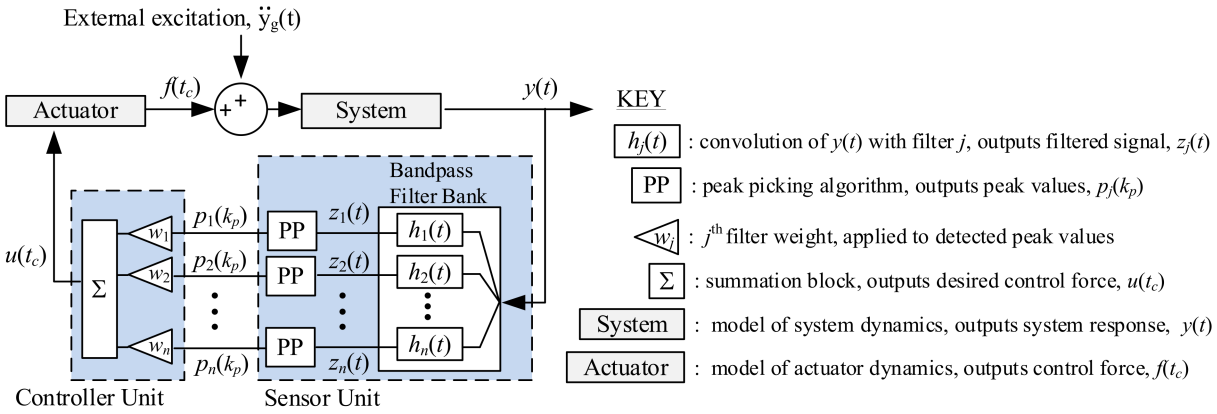

Figure 2. Control architecture using the weighted sum of peaks from the filtered system response.

There is no empirical method for determining the parameters in the control weighting vector, $\hat{W}$, as shown in [25], and the PSO is one option for determining these control parameters. In the PSO optimization technique, each particle represents a potential weighting vector, $\hat{W}$, where $\hat{W} = [w_1\ w_2\ \cdots\ w_n]$. After completing the optimization, the particle with the smallest fitness function is chosen as the resulting weighting vector. This optimization is completed offline and prior to the control event, thereby minimizing the computational demand on the actuating node during the actual seismic event.

4. Application of Control Parameter Optimization on Five-Story Benchmark Structure

To validate the PSO-H optimization on the control weighting vector, the five-story Kajima-Shizouka building was used as a benchmark structure (Figure 3). All simulations were executed using MATLAB. The structure was modeled as a lumped mass system, similar to that proposed by [32], which is based on the actual structure used in the study conducted in [33]. The structural properties are given in Table 1, yielding five natural frequencies of 1.00, 2.82, 4.49, 5.80, and 6.77 Hz. The damping in the structure was modeled as a 5% damping ratio based on Rayleigh damping that is both mass-proportional and stiffness-proportional [34]. It is assumed that only the horizontal degrees-of-freedom is measurable and controllable. Each floor is assumed to include an installed transducer, which measures inter-story displacement, and an ideal actuator, which is capable of supplying the demanded control force. In other words, the actuator block in Figure 2 is set to a value of one and $u(t_c)$ equals $f(t_c)$.

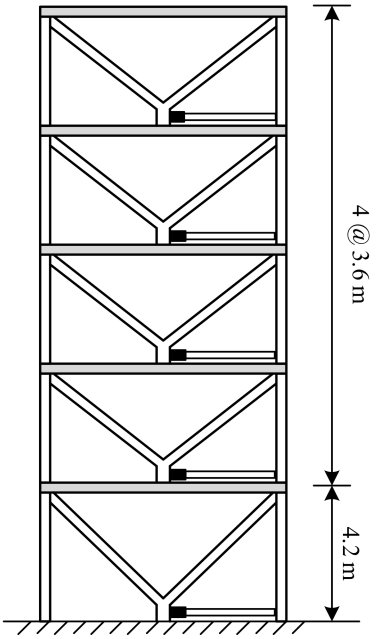

Figure 3. Five-Story Kajima-Shizouka building used as a benchmark structure.

Table 1. Benchmark structure properties.

Floor	Seismic Mass (kg)	Inter-Story Stiffness (kN/m)
1	215.2×10^3	147×10^3
2	209.2×10^3	113×10^3
3	207.0×10^3	99×10^3
4	204.8×10^3	89×10^3
5	266.1×10^3	84×10^3

The base-excited structural system is modeled in continuous time as an m degree-of-freedom, linear time-invariant, lumped mass shear structure. This can be generalized through m equations of motion [34]:

$$M\ddot{y}(t)+C_d\,\dot{y}(t) + K_s y(t) = -M\iota\ddot{y}_g(t) + lf\,(t), \tag{9}$$

where M, C_d, and $K_s\ \epsilon\ \mathbb{R}^{mxm}$ are the mass, damping and stiffness matrices, respectively. The displacement vector relative to the base of the structure is $y\ \epsilon\ \mathbb{R}^m$, $\ddot{y}_g$ is the ground acceleration, and $l\ \epsilon\ \mathbb{R}^m$ is the ground acceleration influence vector, where each term takes

a value of one. The locations of the actuators are described by the matrix $l \epsilon \mathbb{R}^{mxp}$ and $f \epsilon \mathbb{R}^{p}$ is a vector of control forces given that p is the number of input control forces. The variable t represents continuous time. By setting the control force, $\boldsymbol{f}$, equal to zero, the uncontrolled response of the structure to the base excitation is approximated using the integration method proposed by Newmark [34]. In this simulation, the control frequency was set to 100 Hz and the simulation time-step was 488 µsec. It is assumed that the control force is held constant in between control time-steps.

To introduce the weighted-sum control algorithm, it is assumed that each floor is outfitted with a bank of bandpass filters that are optimized to fully capture the displacement signal of that floor. Previous parametric studies have shown that a sensor with 11 filters, each having a center frequency every 0.7 Hz and a passband of 0.5 Hz, is optimal for representing the response of the structure to seismic base excitation [30]. The dynamics of each filter is modeled using Equations (5) and (6). It is assumed that every unit in the filter bank is able to broadcast the peaks from its filtered signal to the controller on each floor and therefore every filter on every floor in the filter bank has a weighted connection with every controller on every floor. For the five-story structure, this resulted in a weight matrix, $\boldsymbol{W}$, that was 55 × 5 elements. The 55 rows in this matrix were derived from five sensors, each having eleven filters, and the five columns were due to the connections with the five actuators (Figure 4). For the PSO algorithm, this matrix was rearranged into a 275-element particle and when represented in vector format, it is termed $\hat{W}$.

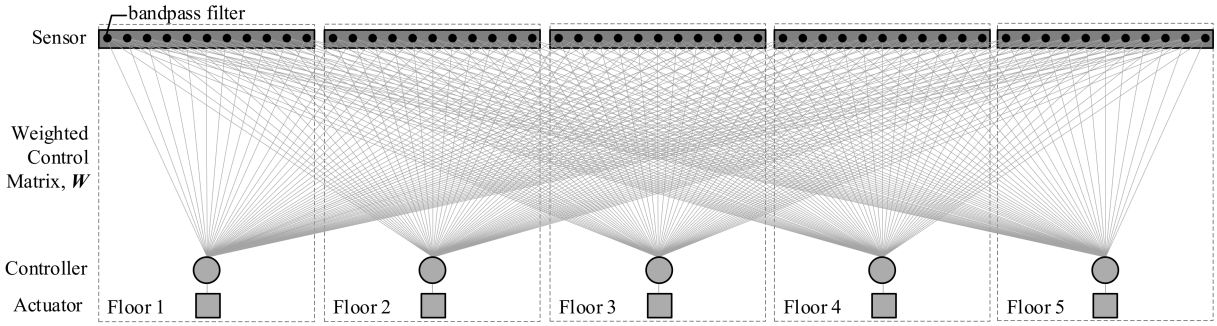

Figure 4. Visual representation of the connections between sensors and controllers; each line between the sensor and controller represents weighted information exchange.

In order to optimize the weighting vector for the purposes of control using PSO, a viable fitness function is needed. Several cost functions that were proposed in [35] were used as a measure for quantifying the effectiveness of control for a given weighting vector. These metrics are chosen as they offer a dimensionless quantification, which makes them easily adaptable to a fitness function for the PSO algorithm and they have been used in numerous other studies, for example, in [8,25], and [36]. Two of these cost functions focus on minimizing the inter-story drift of the structure, which reduces the likelihood of damage to the building system. One of these cost functions quantifies the reduction of the absolute maximum drift, expressed as

$$J_1 = \frac{\max(|d(t)_{controlled}|)}{\max(|d(t)_{uncontrolled}|)}, \tag{10}$$

and the other cost function quantifies the overall time history reduction of the inter-story drift, expressed as

$$J_2 = \frac{d(t)_{controlled}}{d(t)_{uncontrolled}}. \tag{11}$$

In these equations, $d(t)_{uncontrolled}$ is the time history of the inter-story drift for all floors without any implementation of control, while $d(t)_{uncontrolled}$ represents the response of the structure when subject to a control scenario. Furthermore, $|\cdot|$ is the absolute value function

and $\|\cdot\|$ denotes the l_2-norm function. The other two cost functions focus on minimizing the acceleration of the structure, which is related to the occupational comfort during the event. Similar to the displacement cost functions, the acceleration cost functions quantify the reduction of the absolute maximum acceleration, $\ddot{y}(t)$, expressed as

$$J_3 = \frac{\max\left(\left|\ddot{y}(t)_{controlled}\right|\right)}{\max\left(\left|\ddot{y}(t)_{uncontrolled}\right|\right)}, \tag{12}$$

and the time history response, expressed as

$$J_4 = \frac{\ddot{y}(t)_{controlled}}{\ddot{y}(t)_{uncontrolled}}. \tag{13}$$

The demanded control force is also quantified through a cost function provided in [35], which is defined as

$$J_5 = \frac{\max(|f(t)|)}{W_s}, \tag{14}$$

where $f(t)$ is the time history of the control force for each floor and W_s is the seismic weight of the building based on the above ground mass of the structure.

Each cost function is a m-dimensional vector, where m is the number of floors in the structure, thereby providing quantification for each floor in the structure. As the PSO algorithm, in general, requires a single fitness function, these five resulting vectors are summed together across all floors, yielding

$$O = \sum_{l=1}^{m} J_{1,l} + J_{2,l} + J_{3,l} + J_{4,l} + 5J_{5,l}\ . \tag{15}$$

In an uncontrolled scenario, the first four cost functions, J_1 to J_4, each take on a value of 1.0 for all floors, which sums to 20 for the five-story structure. It is observed that J_5 typically takes on values of 0.2 or less for each floor in this simulation in order for it to be an equally weighted objective and a scalar of 5.0 is included with this cost function. Therefore, if the fitness function is less than 25, it can be concluded that the weight matrix is effective, as the uncontrolled response is likely less than the controlled response.

To determine the optimal weight matrix, W, the five-story structure was subject to seismic base excitation in simulation using the 1940 El Centro (SE) earthquake ground acceleration record (Figure 5). The dynamics of the structure and the associated sensing nodes were modeled using Equations (4)–(7) and (9), and the response of the structure to the excitation was approximated using the Newmark integration method [34]. To cover an adequate search space, the algorithm uses 50 particles. To confirm convergence of the algorithm, the particles are trained until the best solution, $\boldsymbol{g}$, does not change for 50 consecutive iterations. This does not ensure locating a global minimum, but with an adequate number of particles and with executing the homing feature, the algorithm does locate a competitive local minimum. Using these metrics, the weight matrix is trained using the PSO-H algorithm, resulting in the cost functions shown in Table 2, denoted as Weighted-sum in the table. A sample time history response for the drift is shown in Figure 6. To ensure that the weight matrix is not over-trained to the El Centro record, it is also validated using the 1995 Kobe (NS JMA) and 1989 Loma Prieta (CORRALITOS) earthquake ground acceleration records (Figure 5). These results are shown in Tables 3 and 4.

As a comparison to the weighted-control algorithm, a traditional full-state feedback linear quadratic regulator (LQR) [37] was also considered. This controller assumes that all necessary states (i.e., displacement and velocity) of all floors are measurable or estimates them using techniques such as the Kalman filter.

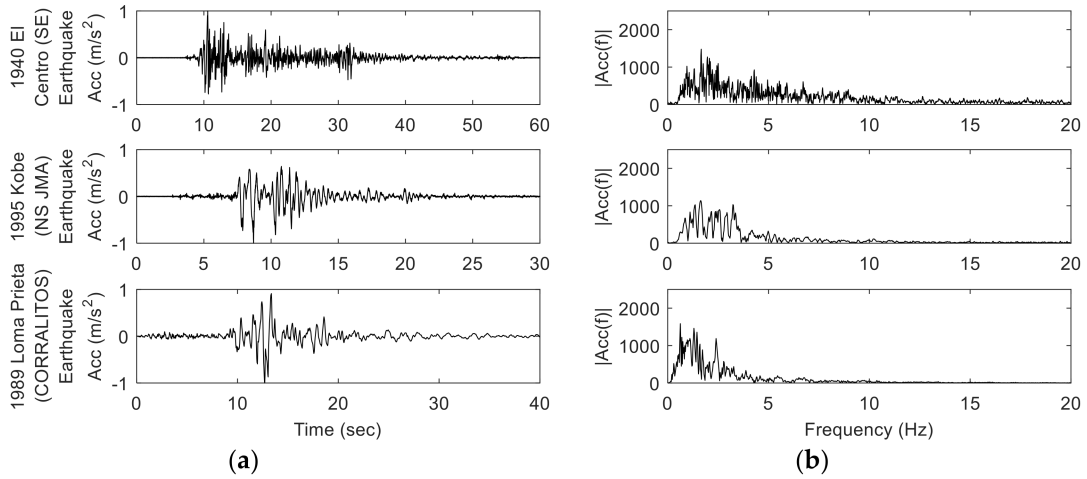

Figure 5. Seismic signals used as base excitation in the simulation in time (**a**) and frequency (**b**) domains. Abbreviations: SE, southeast; NS, north–south; and JMA, Japan Meteorological Agency.

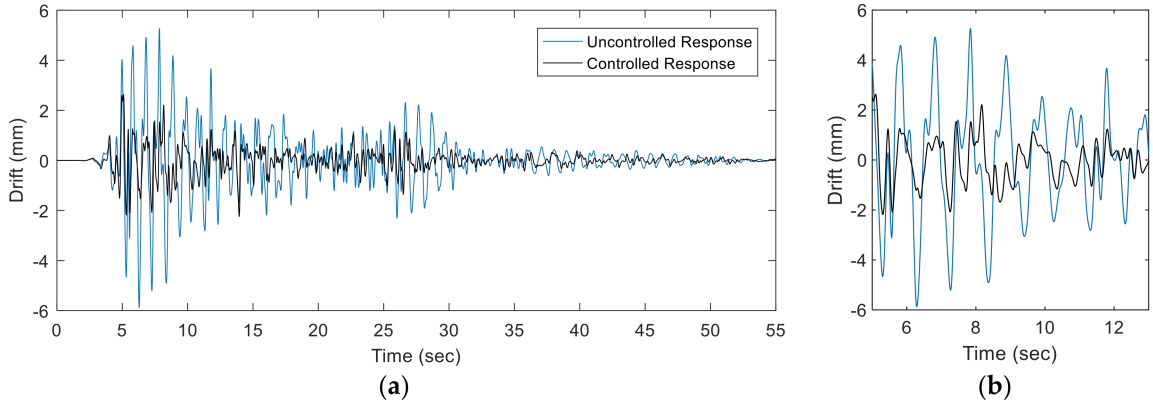

Figure 6. Inter-story drift response of the fifth floor when subject to the El Centro earthquake, shown on a full-time scale (**a**) and sub-section of time (**b**).

The LQR uses the algebraic Ricatti equation to minimize the cost function

$$J = \int_0^\infty (\overline{y}^{\mathrm{T}} Q \overline{y} + u^{\mathrm{T}} R u) dt \tag{16}$$

subject to the full state feedback control law, expressed as u = -K, where $\overline{y} \epsilon\ \mathbb{R}^{1\times 2m} = \begin{bmatrix} y\ \dot{y} \end{bmatrix}$ is a vector of the inter-story displacement and velocity of all the floors of the structure and $K\ \epsilon\ \mathbb{R}^{p\mathrm{x}2m}$ is the resulting constant feedback gain matrix, given m states (or floors) and p control forces.

This minimization is subject to two parameters: $Q\ \epsilon\ \mathbb{R}^{2m\mathrm{x}2m}$, which applies a weight to the cost of the structural response and $R\ \epsilon\ \mathbb{R}^{p\mathrm{x}p}$, which applies a weight to the cost of the control effort. In the algorithm, Q and R are chosen using the commonly accepted Bryson's Rule [38] that establishes these values as proportional to the inverse of the square of the maximum acceptable displacement and control force, respectively. For this application, the non-zero entries of Q are 10^{10} and the non-zero entries of R are $10^{-5.4}$. Based on limitations described in [7], it is assumed that the control sampling frequency is limited to 40 Hz, which subjects the control effort to realistic experimental constraints.The results from this controller are shown in Tables 2–4 for the El Centro, Kobe, and Loma Prieta earthquakes.

Table 2. Cost functions J_1 through J_6 for El Centro earthquake. Bold indicates the cost function that yields the minimum cost function for each floor.

Control Scenario \ Floor		1	2	3	4	5
J_1	Weighted-sum	0.359	0.425	0.468	0.452	0.385
	Weighted-sum–220	**0.347**	0.413	0.451	0.401	0.347
	LQR	0.415	**0.350**	**0.318**	**0.306**	**0.305**
J_2	Weighted-sum	0.305	0.300	0.320	0.341	0.392
	Weighted-sum–220	0.293	0.288	0.306	0.298	0.328
	LQR	**0.237**	**0.199**	**0.195**	**0.200**	**0.204**
J_3	Weighted-sum	0.841	0.815	0.789	0.803	0.679
	Weighted-sum–220	**0.757**	**0.787**	**0.712**	**0.750**	**0.661**
	LQR	1.024	0.932	0.868	0.918	0.703
J_4	Weighted-sum	0.743	0.687	0.693	0.634	0.564
	Weighted-sum–220	0.741	0.686	0.666	0.610	0.533
	LQR	**0.701**	**0.581**	**0.518**	**0.468**	**0.413**
J_5	Weighted-sum	0.055	**0.045**	0.081	**0.064**	0.152
	Weighted-sum–220	0.077	0.102	**0.075**	0.066	**0.145**
	LQR	**0.052**	0.077	0.119	0.153	0.178
J_6	Weighted-sum: LQR			1.284		
	Weighted-sum–220: LQR			0.806		

Table 3. Cost functions J_1 through J_6 for Kobe earthquake. Bold indicates the cost function that yields the minimum cost function for each floor.

Control Scenario \ Floor		1	2	3	4	5
J_1	Weighted-sum	0.541	0.497	0.566	0.483	0.511
	Weighted-sum–220	0.526	0.464	0.565	0.438	0.458
	LQR	**0.392**	**0.318**	**0.325**	**0.287**	**0.262**
J_2	Weighted-sum	0.510	0.510	0.539	0.518	0.521
	Weighted-sum–220	0.499	0.491	0.518	0.469	0.458
	LQR	**0.348**	**0.295**	**0.285**	**0.276**	**0.261**
J_3	Weighted-sum	0.810	0.858	0.914	0.924	0.669
	Weighted-sum–220	0.909	0.854	0.909	0.753	0.634
	LQR	**0.757**	**0.727**	**0.659**	**0.533**	**0.412**
J_4	Weighted-sum	0.768	0.650	0.776	0.843	0.707
	Weighted-sum–220	0.760	0.637	0.754	0.856	0.684
	LQR	**0.542**	**0.488**	**0.522**	**0.556**	**0.451**
J_5	Weighted-sum	0.067	**0.048**	**0.087**	**0.080**	0.245
	Weighted-sum–220	0.090	0.097	0.102	0.097	**0.202**
	LQR	**0.042**	0.072	0.105	0.141	0.174
J_6	Weighted-sum: LQR			1.044		
	Weighted-sum–220: LQR			0.525		

The weighted-sum control algorithm has similar control effectiveness as the LQR algorithm when considering the El Centro earthquake for all cost functions (Table 2). However, the LQR controller is much more adaptable to other earthquakes as demonstrated by its continued effectiveness at mitigating inter-story displacement and acceleration for both the Kobe and Loma Prieta earthquakes. The weighted-sum control algorithm is able to reduce the displacement measures (i.e., J_1 and J_2) when the structure is subject

to the other Kobe and Loma Prieta earthquakes, but it is significantly less effective at reducing the acceleration measures (i.e., J_3 and J_4) when compared to the LQR controller (Tables 3 and 4). In application, retraining the weight matrix for the characteristics of the anticipated seismic response could improve the performance of the control algorithm. For all control scenarios, the controllers were more effective at reducing displacement than acceleration, which is typically a trade-off when controlling structures during seismic events. For all earthquakes, the weighted-sum control algorithm did place minimal demand on the actuators, as denoted by the J_5 cost function, and this will contribute to its decrease in control effectiveness.

Table 4. Cost functions J_1 through J_6 for Loma Prieta earthquake. Bold indicates the cost function that yields the minimum cost function for each floor.

Control Scenario \ Floor		1	2	3	4	5
J_1	Weighted-sum	0.414	0.383	0.364	0.360	0.614
	Weighted-sum–220	0.386	0.379	0.326	0.302	0.514
	LQR	**0.286**	**0.226**	**0.204**	**0.213**	**0.222**
J_2	Weighted-sum	0.468	0.449	0.446	0.490	0.613
	Weighted-sum–220	0.454	0.439	0.421	0.456	0.514
	LQR	**0.241**	**0.201**	**0.191**	**0.189**	**0.187**
J_3	Weighted-sum	1.030	0.465	0.579	0.671	0.696
	Weighted-sum–220	1.252	0.463	0.597	0.637	0.601
	LQR	**0.459**	**0.366**	**0.423**	**0.399**	**0.367**
J_4	Weighted-sum	0.975	0.631	0.593	0.519	0.492
	Weighted-sum–220	0.873	0.621	0.573	0.496	0.443
	LQR	**0.395**	**0.327**	**0.295**	**0.273**	**0.257**
J_5	Weighted-sum	0.123	0.129	0.143	**0.161**	0.477
	Weighted-sum–220	0.154	0.225	0.179	0.295	0.400
	LQR	**0.060**	**0.094**	**0.141**	0.179	**0.222**
J_6	Weighted-sum: LQR			1.45		
	Weighted-sum–220: LQR			1.00		

As communication overhead is a common challenge associated with WSUs and in particular when applied to control applications, an additional cost function,

$$J_6 = \frac{NP_1}{NP_2}, \tag{17}$$

is introduced that compares the amount of data that is transmitted during the execution of the weighted-sum control algorithm versus the amount of data that is transmitted during the execution of the traditional LQR algorithm. In this cost index, NP_1 is the number of peaks that are detected from all filters across all floors. NP_2 is the number of data points obtained via traditional Nyquist sampling rates, combined across all floors. While the weighted-sum method does use asynchronous sampling to generate the number of peaks, the bandpass filters decompose the displacement of each floor into eleven signals that must be transmitted, albeit as peaks, to the controller nodes. For all three earthquakes, this resulted in an undesirable increase in information flow, as indicated by J_6 being greater than 1.0 (Tables 3–5). It is hypothesized, however, that not all connections are needed in the weight matrix and some filters can be eliminated from the algorithm. This in turn would reduce the information flow and address one of the common challenges associated with control using WSUs.

Table 5. Percent difference in the fitness function, O2, from the full-state weight matrix for three difference earthquakes.

Method	El Centro EQ	Kobe EQ	Loma Prieta EQ
Minimal-value deletion pruning–220	−5.27%	−3.85%	−5.71%
Minimal-value deletion pruning–230	−1.93%	3.27%	0.15%

5. Integration of Pruning for Stream-Lined Control

As previously noted, the weighted control matrix has high dimensionality ($W \epsilon \mathbb{R}^{55x5}$) and can assume a large range of values (Figure 7). It is hypothesized that due to the high connectivity, not all weight values within the matrix are necessary and some can be removed. This hypothesis is based on experiences with artificial neural networks (ANNs), which share a similar architecture to the proposed weighted-control algorithm. Similar to the structure of the weighted-control algorithm, ANNs typically need to predefine the network architecture, which can cause over-fitting if too many weights are defined or under-fitting if not enough weights are defined. Numerous methods exist for eliminating or pruning the weights in ANNs, such as minimal-value deletion [39], ref [40] that focus only on the magnitude or other methods that develop criteria to assess the importance of the weight [41–44]. The architecture of the proposed control method is more basic than a traditional ANN, only having a single layer of weights and, as a result, some of the elimination criteria in these studies is overly complex. As such, three methods are explored: (1) minimal-value deletion [39], (2) optimal brain surgeon (OBS) [41], and (3) a brute force method, termed minimum error pruning.

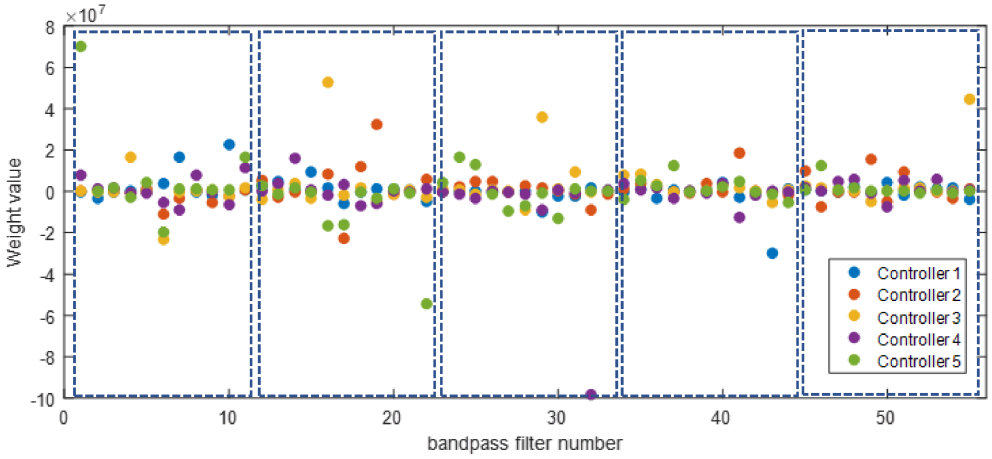

Figure 7. Pictorial representation of values of the weighted control matrix, $W \epsilon \mathbb{R}^{55x5}$. Note: bandpass filter numbers $11 \times l - 10$ to $11 \times l$ correspond to the filters on the lth floor.

With each method, the effect of the minimized weighted control matrix is evaluated using the percent change in the fitness function,

$$C = \frac{O_{2,1} - O_{2,0}}{O_{2,0}} * 100\%, \quad (18)$$

where C is the percent difference, $O_{2,1}$ is the fitness function after implementing a pruning method, and $O_{2,0}$ is the original fitness function from the PSO-H optimization using the El Centro earthquake record, both of which use a modified fitness function (Equation (19)). As the weighted control matrix becomes sparse, it is possible for all connections to be eliminated to an actuator. When this occurs, elements of the J_5 cost function become zero while the displacement or acceleration of the structure may be undesirably increasing. As a

result, a modified fitness function is used for the assessment of the effectiveness of the pruning method that omits the control force cost function (i.e., J_5),

$$O_2 = \sum_{l=1}^{m} J_{1,l} + J_{2,l} + J_{3,l} + J_{4,l}. \tag{19}$$

The effectiveness of the pruning algorithms was also evaluated using the number of removed weights and the number of removed filters. A filter is removed when it is no longer connected to any of the five controllers, indicating that its information is not required for any of the control force calculations. It is the removal of a filter, rather than just a weight, that is most beneficial to the network as it results in less information exchange across the network, which translates to power savings and also a more streamlined control-force calculation at the controller.

The first pruning method that was considered is a minimal-value deletion algorithm that eliminates a single weight with each iteration of the algorithm based on its magnitude [39]. For this algorithm, the weight with the smallest absolute magnitude is eliminated and the fitness function is evaluated for the reduced weighted control matrix. The process is repeated for the weight with the second smallest absolute magnitude. This elimination of weights continues until 270 weights have been eliminated and only five weights remain. The resulting percent change in the fitness function as a function of the removed weights is shown in Figure 8a. The resulting number of removed filters as a function of removed weights is shown in Figure 8b.

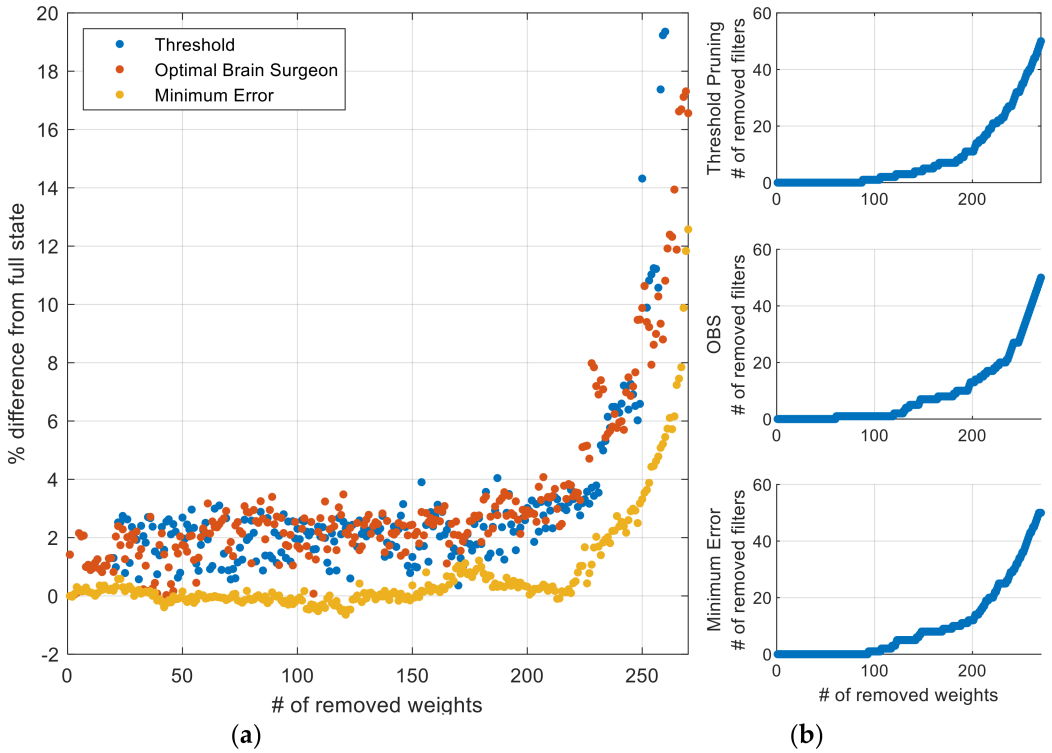

Figure 8. Percent difference in the fitness function from the unpruned, full-state weighted control matrix for the three pruning methods ((**a**), note that a negative value indicates an improved performance) and the total number of filters removed through pruning (**b**).

Next, the optimal brain surgeon (OBS) algorithm was considered [41]. OBS uses the Hessian matrix, H, to create a vector of saliencies, L, where each qth entry in the vector is defined as

$$L_q = \frac{1}{2} \frac{w_q^2}{[H^{-1}]_{qq}}, \tag{20}$$

given that w_q is the qth weight in the weight vector, $\hat{W}$. The inverse Hessian matrix is calculated as

$$H_{r+1}^{-1} = H_r^{-1} - \frac{H_r^{-1} \cdot X^{[r+1]} \cdot X^{[r+1]T} \cdot H_r^{-1}}{X^{[r+1]} \cdot X^{[r+1]T} \cdot H_r^{-1}}, \tag{21}$$

such that $(\cdot)^{-1}$ is the inverse function, r is the iteration number, and $\boldsymbol{X}$ is a vector of partial derivatives. As the standard application of OBS is for multi-layer networks, $\boldsymbol{X}$ is truncated to only include derivatives with respect to the input-to-output layers, similar to the hidden-to-output weights discussed in [41]. For the weighted control algorithm, the output layer uses a linear activation function, which reduces it down to $X^{[r]T} = \hat{W} * z(r)$, where $z(r)$ is the output of the bandpass filters on the rth iteration. In this instance, the number of iterations equals the number of time-steps in the simulation.

As specified in [41], the weight with the smallest saliency is used to update all other weights by deriving a weight change vector,

$$\delta w = -\frac{w_q}{[H^{-1}]_{qq}} H^{-1} \cdot e_q \,, \tag{22}$$

and adding this to the weight vector, $\hat{W}$. In Equation (22), e_q is the unit vector in weight space corresponding to the qth weight w_q. After updating all weights, the identified weight is removed from the matrix. The algorithm continues to eliminate weights in this manner until there is an unacceptable amount of incurred error, at which point the network could be retrained. To understand the effect of removing weights, the stopping error for the algorithm was incrementally increased without implementing any retraining until 270 weights had been removed. The resulting percent change in the objective function as a function of the removed weights is shown in Figure 8a. The resulting number of removed filters as a function of the removed weights is shown in Figure 8b.

Finally, the third method that was considered for eliminating extraneous weights is the minimum error method. In this method, one weight is temporarily removed and the reduced weighted control matrix is evaluated using the fitness function (Equation (19)). This weight is then inserted back into the matrix, the next weight is removed, and the fitness function is evaluated. After all weights are considered, the weight that results in the smallest fitness function is permanently removed. This is repeated for all remaining weights until 270 weights have been removed. The resulting percent change in the fitness function as a function of the removed weights is shown in Figure 8a. The resulting number of removed filters as a function of the removed weights is shown in Figure 8b.

As can be seen from Figure 8a, there is a non-linear relationship between the weights and the fitness function for all three methods. In particular, up to 223 weights can be removed for any of the three methods and less than a 5% degradation in control effectiveness occurs when comparing the full state to the pruned state. After that, the percent difference rapidly increases for the minimal-value deletion pruning and OBS methods. The minimum error pruning method, however, only incurs 1.03% error with 223 removed weights and 257 weights can be removed while still incurring less than 5% error. Another interesting trend is that the percent change in all three methods did not always incrementally increase. In some instances, removing additional weights actually improved the performance of the network. This was particularly true for the minimal-value deletion pruning and OBS, but was still evident to a smaller extent in the minimum error method. The minimum error method significantly outperformed the other two methods and, in some cases, a negative percent change was observed, indicating that the pruned network performed better than the full-state network. The pruned states resulting from minimal-value deletion pruning and OBS never performed better than the full-state network.

When considering the number of removed filters versus the number of removed weights (Figure 8b), all three methods exhibited very similar trends. Initially, the number of removed filters remained at zero, even as the number of removed weights increased, because a filter was only removed when it was no longer connected to any controller units.

However, once a significant portion of weights have been removed, the number of removed filters rapidly increases as connections are removed. Removing filters is a competing metric with the incurred error, as shown in Figure 8a. It is desirable to remove more filters as this results in a more streamlined control algorithm, but as more filters are removed, the control effectiveness degrades as indicated by an increase in percent error. Therefore, determining the optimal number of weights to remove is a balance between these two metrics and requires some subjectivity.

Pruning Methods with Periodic PSO-H Retraining

While the error that incurred through the removal of weights was relatively small, it was next considered whether the control effectiveness could be improved by periodically retraining the weighted control matrix using the PSO-H algorithm during the three pruning processes. Each pruning method was re-executed with the modification that once groups of 10 weights have been removed, the weighted control matrix was retrained. The PSO-H-retraining algorithm continued to use 50 particles, with each particle also eliminating the weights that were identified through the pruning mechanism. At the start of each retraining session, λ, the inertia weight from Equation (3), was reset to 1.0 to allow the search to start globally and move locally. The PSO-H algorithm iterates until the best fitness function does not change for 50 iterations. The retraining pruning algorithms were compared against the control effectiveness of the full-state network, each using the El Centro earthquake for seismic excitation. The resulting percent change from the full-state network is shown in Figure 9a for the three different pruning methods. For comparison, the pruning methods without retraining, extracted from Figure 8a, are also overlain on the figure.

In general, all three pruning methods showed improvement over the full-state matrix when including periodic retraining. In contrast to the pruning without retraining, the OBS and minimal-value deletion methods now outperformed the minimum error method and were able to improve the control effectiveness when compared to the full-state matrix by over 6% in some cases. The pruned network produced the best results when using minimal-value deletion pruning to eliminate 170 weights, with a 6.28% improvement in control effectiveness. However, this only resulted in eliminating six filters, which did not streamline data communication. When 220 weights were removed using Minimal-value deletion pruning, this still maintained an improved control effectiveness, with 5.27% difference, and also eliminated 20 filters or an approximate reduction of 36.4% in the data transmission (=20 removed filters/55 total filters). Removing 230 weights is also attractive as it improves control effectiveness, though less with a 1.93% difference, and now eliminates 28 filters or an approximate reduction of 50.9% in the data transmission (Table 5). The OBS method performed similarly to the minimal-value deletion pruning method but was not able to achieve the same improvement in control effectiveness and therefore was not considered in more detail. The minimum error method was able to improve when integrated into periodic retraining but contrary to the results without retraining, its performance lagged behind the minimal-value deletion and OBS methods.

To once again ensure that the pruned weighted control matrix was not over-trained to the El Centro earthquake, the matrices that were pruned using minimal-value deletion pruning for 220 weights and 230 weights were applied to control the structure when subject to the 1995 Kobe (NS JMA) and 1989 Loma Prieta (CORRALITOS) earthquake ground acceleration records (Table 5). When removing 220 weights, the remaining weights allowed for enough generality that effective control could still be achieved for these two earthquakes, as indicated by the negative percent change in the fitness function. When removing 230 weights, however, the remaining weights were less effective at controlling the structure and some degradation in the control began to be apparent, perhaps indicating overfitting. Therefore, removing 220 weights using the minimal-value deletion pruning method is chosen as the optimal scenario as it is effective at controlling the structure but still remains generalizable to multiple input earthquakes.

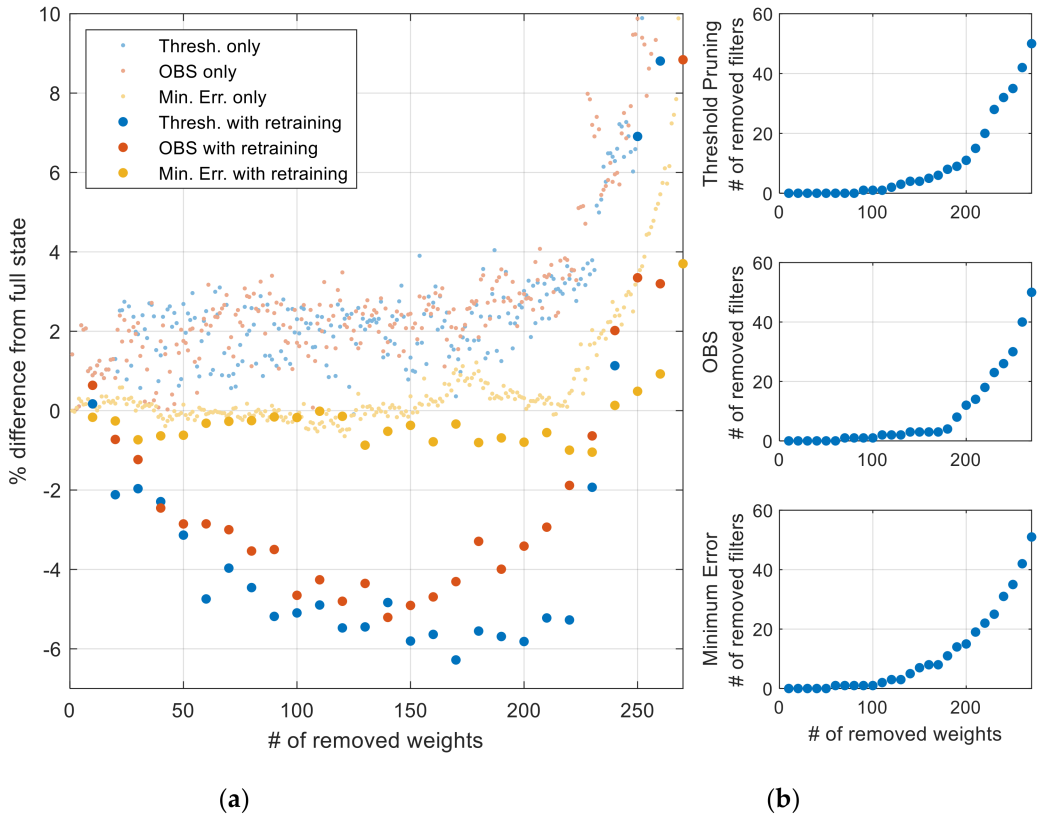

Figure 9. Percent difference in the fitness function from the unpruned, full-state weight matrix for the three pruning methods, with each pruning method without retraining overlain for comparison ((**a**), note that a negative value indicates an improved performance), and the total number of filters removed through pruning (**b**).

The full results for all cost functions using the minimal-value deletion pruning for 220 weights are shown in Tables 2–4. In almost all cost functions and for all earthquakes, the pruned matrix outperformed the full-state matrix and was closer to the performance of the LQR controller. Similar to the full-state controller, the pruned control scheme is not as adaptable to the Kobe and Loma Prieta earthquakes. However, across all earthquakes, this controller scheme places more demand on the actuators, which likely contributes to its increase in control effectiveness. The pruned matrix showed the most promise, though, in addressing the communication challenges of the network. For the El Centro earthquake, the pruned method transmitted 19.4% less data than the LQR and for the Kobe, it transmitted 47.5% less data. The two methods transmitted equal amounts of data for the Loma Prieta earthquake.

6. Conclusions

While integration of feedback control systems into civil infrastructure is not a new area of research, several challenges of the technology, such as computational delays and communication constraints, have prevented their widespread adoption. This study proposes using a control algorithm that leverages front-end signal processing to enable streamlined control at the actuation node and has the potential to overcome many of these challenges. The control algorithm reduces down to a simplistic weighted combination of the inputs that can easily be implemented in real-time on a controller node. The weights of this algorithm were initially developed using the particle swarm optimization with a homing feature (PSO-H) on a five-story benchmark structure. To further streamline the computations for the control algorithm and reduce unnecessary data-sharing, three pruning methods were employed, with the minimum error method resulting in increased control effectiveness through the elimination of extraneous weights. As weights were removed using this method, however,

the remaining control parameters were no longer optimized and therefore the pruning methods were re-executed with periodic retraining using the PSO-H algorithm. This resulted in a pruned weight matrix using minimal-value deletion pruning that produces more effective control while also reducing the amount of transmitted data by 19.4%.

With the validation of the PSO algorithm and integrated pruning techniques in simulation, future work will include the experimental validation of the proposed weighted-sum control algorithm. This future step is critical in validating the real-time control of the proposed control process and the streamlined communication capabilities. To achieve this, the proposed control process will be applied to a small-scale, multi-story laboratory structure that is placed on a single degree-of-freedom shake table. The structure is outfitted with transducers for measuring inter-story displacement and actuators for mitigating the effect of seismic base excitation. Information about the displacement of the structure will be acquired by the novel sensing node developed in [30] and the peaks from the real-time spectral components will be transmitted to a secondary sensing unit that both serves as the controller and executes the weighted-sum control algorithm. Prior to implementation, the weighting matrix will be determined for this new structure using the PSO-H algorithm. A comparative baseline method, such as LQR, will also be implemented on this set-up. Both the proposed control algorithm and the comparative baseline algorithm will face challenges that were not addressed in this study. First, the limitations of the wireless telemetry naturally result in lost data packets, which can degrade the control effectiveness. Accounting for this limitation in this study was attempted through carefully chosen time sampling schemes but experimental validation is necessary to fully validate this. Second, this study assumed an ideal actuator with no limitations or dynamics. The actual actuator dynamics will also affect the control time-step and place limitations on the amount of force that can be applied. Therefore, while this study was a successful numerical application of the proposed control algorithm, a necessary next step is experimental validation.

Author Contributions: Conceptualization, C.A.P.; methodology, C.A.P. and A.A.; software, C.A.P., A.A. and C.F.; validation, C.A.P.; formal analysis, C.A.P. and C.V.; investigation, C.A.P. and M.C.N.; resources, C.A.P.; data curation, C.A.P.; writing—original draft preparation, C.A.P.; writing—review and editing, C.A.P., M.C.N., C.V.; visualization, C.A.P.; supervision, C.A.P.; project administration, C.A.P.; funding acquisition, C.A.P. All authors have read and agreed to the published version of the manuscript.

Funding: This research was funded by the National Science Foundation (NSF), grant number CMMI-1662655.

Data Availability Statement: Raw data were generated at Hope College. Derived data supporting the findings of this study are available from the corresponding author (C.A.P.) on request.

Acknowledgments: The authors gratefully acknowledge the support of the Clare Boothe Luce Program of the Henry Luce Foundation.

Conflicts of Interest: The authors declare no conflict of interest. The funders had no role in the design of the study; in the collection, analyses, or interpretation of data; in the writing of the manuscript, or in the decision to publish the results.

Nomenclature

C	Percent change in fitness function	C_d	damping matrix of structure
H	Hessian matrix	H_0	filter gain
$H_j(s)$	jth bandpass filter transfer function	J	LQR cost function
J_1–J_6	Control cost functions	K	LQR feedback gain matrix
K_s	Stiffness matrix of structure	L	saliency (OBS)
M	Mass matrix of structure	O	fitness function for PSO
NP_1	Number of transmitted peak values	NP_2	number of transmitted data points
P	Vector of detected peak values for all filters	$Q_{0,j}$	frequency selectivity of each jth filter
Q	LQR parameter that weighs the cost of the structural response	R	LQR parameter that weighs the cost of the control effort
U	Control force	W	control weighting matrix
$\widehat{W}$	Control weighting vector	X	vector of partial derivative (OBS)
d	Inter-story drift vector of all floors	e	unit vector in weight space (OBS)
$f(t)$	Control force output from actuator	g	best position of all particles (PSO)
$h_j(t)$	Impulse response of the j^{th} filter	l	actuator location matrix
ι	Ground acceleration influence vector	t	continuous time
t_c	Control time increment	x	current position of a particle (PSO)
x_b	Previous best position of a particle (PSO)	x_g	ground displacement
y	Displacement of structure	$\overline{y}$	states of the system (i.e., inter-story displacement and velocity for all floors of the structure)
$z_j(t)$	Output of the jth bandpass filter	γ_1, γ_2	acceleration coefficients (PSO)
ρ_1, ρ_2	Random number between 0 and 1 (PSO)	λ	inertia weight (PSO)
τ	Inertial damping constant (PSO)	δ_ω	weight change vector (OBS)
ξ	Filter damping ratio	ω	filter center frequency

References

1. Yao, J.T.P. Concept of structural control. *J. Struct. Div.* **1972**, *98*, 1567–1574. [CrossRef]
2. Housner, G.W.; Bergman, L.A.; Caughey, T.K.; Chassiakos, A.G.; Claus, R.O.; Masri, S.F.; Skelton, R.E.; Soong, T.T.; Spencer, B.F.; Yao, J.T.P. Structural control: Past, present, and future. *J. Eng. Mech.* **1997**, *123*, 897–971. [CrossRef]
3. Spencer, B.F.; Nagarajaiah, S. State of the art of structural control. *J. Struct. Eng.* **2003**, *129*, 845–856. [CrossRef]
4. Soong, T.T. *Active Structural Control: Theory and Practice*; Longman Scientific & Technical: London, UK; Wiley: New York, NY, USA, 1990.
5. Wang, Y.; Swartz, A.; Lynch, J.P.; Law, K.H.; Lu, K.-C.; Loh, C.-H. Wireless feedback structural control with embedded computing. In *Health Monitoring and Smart Nondestructive Evaluation of Structural and Biological Systems V*; SPIE-Nondestructive evaluation for health monitoring and diagnostics: San Diego, CA, USA, 2006; Volume 6177. [CrossRef]
6. Lynch, J.P.; Wang, Y.; Swartz, R.A.; Lu, K.C.; Loh, C.H. Implementation of a closed-loop structural control system using wireless sensor networks. *Struct. Control. Health Monit.* **2007**, *15*, 518–539. [CrossRef]
7. Spencer, B.F., Jr.; Jo, H.; Mechitov, K.A.; Li, J.; Sim, S.-H.; Kim, R.E.; Cho, S.; Linderman, L.; Moinzadeh, P.; Giles, R.K.; et al. Recent advances in wireless smart sensors for multi-scale monitoring and control of civil infrastructure. *J. Civ. Struct. Health Monit.* **2016**, *6*, 17–41. [CrossRef]
8. Swartz, R.A.; Lynch, J.P. Strategic network utilization in a wireless structural control system for seismically excited structures. *J. Struct. Eng.* **2009**, *135*, 597–608. [CrossRef]
9. Verdoljak, R.; Linderman, L.E. Sparse feedback structures for control of civil systems. *Struct. Control Health Monit.* **2006**, *23*, 1334–1349. [CrossRef]
10. Wang, Y.; Lynch, J.P.; Law, K.H. Decentralized H-infinity controller design for large-scale civil structures. *Earthq. Eng. Struct. Dyn.* **2009**, *38*, 377–401. [CrossRef]
11. Wang, Y.; Law, K.H. Structural control of multi-subnet wireless sensing feedback: Experimental validation of time-delayed decentralized h-infinity control design. *Adv. Struct. Eng.* **2011**, *14*, 25–39. [CrossRef]
12. Štimac, G.; Braut, S.; Žigulić, R. Comparative analysis of PSO algorithms for PID controller tuning. *Chin. J. Mech. Eng.* **2014**, *27*, 928–936. [CrossRef]
13. Guo, R.; Wei, X.-K.; Gao, J. An Improved PID Controller Based on Particle Swarm Optimization for Active Control Engine Mount. 2017. Available online: https://www.sae.org/publications/technical-papers/content/2017-01-1056/ (accessed on 1 September 2021). [CrossRef]
14. De Moura Oliveira, J.P.B.; Hedengren, J.D.; Pires, E.J.S. Swarm-based design of proportional integral and derivative controllers using a compromise cost function: An Arduino temperature laboratory case study. *Algorithms* **2020**, *13*, 315. [CrossRef]

15. Sungthong, A.; Assawinchaichote, W. Particle swam optimization based optimal PID parameters for air heater temperature control system. *Procedia Comput. Sci.* **2016**, *86*, 108–111. [CrossRef]
16. Rodriguez-Abreo, O.; Rodriguez-Resendiz, J.; Fuentes-Silva, C.; Hernandez-Alvarado, R.; Del Consuelo Patricia Torres Falcón, M. Self-tuning neural network PID with dynamic response control. *IEEE Access* **2021**, *9*, 65206–65215. [CrossRef]
17. Zhao, J.; Xi, M. Self-Tuning of PID parameters based on adaptive genetic algorithm. *IOP Conf. Ser. Mater. Sci. Eng.* **2020**, *782*, 042028. [CrossRef]
18. Mahfoud, S.; Derouich, A.; EL Ouanjli, N.; EL Mahfoud, M.; Taoussi, M. A New Strategy-based PID controller optimized by genetic algorithm for DTC of the doubly fed induction motor. *Systems* **2021**, *9*, 37. [CrossRef]
19. Jaen-Cuellar, A.Y.; Romero-Troncoso, R.; Morales-Velazquez, L.; Osornio-Rios, R.A. PID-controller tuning optimization with genetic algorithms in servo systems. *Int. J. Adv. Robot. Syst.* **2013**, *10*, 324. [CrossRef]
20. Hughes, J.E.; Kim, Y.; Chong, J.W.; Kim, C. Particle swarm optimization for active structural control of highway bridges subjected to impact loading. *Shock. Vib.* **2018**, *2018*, 1–12. [CrossRef]
21. Etedali, S.; Tavakoli, S. PD/PID controller design for seismic control of high-rise buildings using multi-objective optimization: A comparative study with LQR controller. *J. Earthq. Tsunami* **2017**, *11*, 1750009. [CrossRef]
22. Heidari, A.H.; Etedali, S.; Javaheri-Tafti, M.R. A hybrid LQR-PID control design for seismic control of buildings equipped with ATMD. *Front. Struct. Civ. Eng.* **2018**, *12*, 44–57. [CrossRef]
23. Baygi, S.M.H.; Karsaz, A. A hybrid optimal PID-LQR control of structural system: A case study of salp swarm optimization. In Proceedings of the 2018 3rd Conference on Swarm Intelligence and Evolutionary Computation (CSIEC), Bam, Iran, 6–8 March 2018; pp. 1–6. [CrossRef]
24. Ulusoy, S.; Nigdeli, S.M.; Bekdaş, G. Novel metaheuristic-based tuning of PID controllers for seismic structures and verification of robustness. *J. Build. Eng.* **2021**, *33*, 101647. [CrossRef]
25. Peckens, C.A.; Cook, I.; Fogg, C. Bio-inspired sensing and actuating architectures for feedback control of civil structures. *Bioinspiration Biomim.* **2019**, *14*, 036008. [CrossRef]
26. Kennedy, J.; Eberhart, R. Particle swarm optimization. In Proceedings of the ICNN'95—International Conference on Neural Networks, Perth, WA, Australia, 27 November–1 December 1995.
27. Shi, Y.; Eberhart, R. A Modified particle swarm optimizer. In Proceedings of the IEEE International Conference on Evolutionary Computation, Anchorage, AK, USA, 4–9 May 1998.
28. Poli, R.; Kennedy, J.; Blackwell, T. Particle swarm optimization: An overview. *Swarm Intell.* **2007**, *1*, 33–57. [CrossRef]
29. Peckens, C.A.; Lynch, J.P. Utilizing the cochlea as a bio-inspired compressive sensing technique. *Smart Mater. Struct.* **2013**, *22*. [CrossRef]
30. Peckens, C.A.; Lynch, J.P.; Heo, G. Resource-efficient wireless sensor network architecture based on bio-mimicry of the mammalian auditory system. *J. Intell. Mater. Syst. Struct.* **2015**, *26*, 79–100. [CrossRef]
31. Zumbahlen, H. Phase Response in Active Filters—Part 3—The Bandpass Response. 2016. Available online: https://www.analog.com/en/analog-dialogue.html (accessed on 24 September 2021).
32. Wang, Y. *Wireless Sensing and Decentralized Control for Civil Structures: Theory and Implementation*; Stanford University: Palo Alto, CA, USA, 2007.
33. Kurata, N. Actual seismic response control building with semi-active damper system. In Proceedings of the Structures Congress 2001, Washington, DC, USA, 21–23 May 2001. [CrossRef]
34. Chopra, A.K. *Dynamics of Structures, Theory and Applications to Earthquake Engineering*, 5th ed.; Pearson Education Limited: Hoboken, NY, USA, 2017.
35. Ohtori, Y.; Christenson, R.E.; Spencer, J.B.F.; Dyke, S. Benchmark control problems for seismically excited nonlinear buildings. *J. Eng. Mech.* **2004**, *130*, 366–385. [CrossRef]
36. Yan, G.; Chen, F.; Wu, Y.-X. A semi-active H∞ control strategy with application to the vibration suppression of nonlinear high-rise building under earthquake excitations. *SpringerPlus* **2016**, *5*, 1–17. [CrossRef]
37. Kalman, R.E. Contributions to the theory of optimal control. *Bol. Soc. Mat. Mex.* **1960**, *5*, 102–119.
38. Franklin, G.F.; Powell, J.D.; Emami-Naeini, A. *Feedback Control of Dynamic Systems*, 7th ed.; Pearson: Boston, MA, USA, 2015.
39. Chechik, G.; Meilijson, I.; Ruppin, E. Synaptic pruning in development: A computational account. *Neural Comput.* **1998**, *10*, 1759–1777. [CrossRef]
40. Han, S.; Pool, J.; Tran, J.; Dally, W.J. Learning both weights and connections for efficient neural networks. *arXiv* **2015**, arXiv:1506.02626.
41. Hassibi, B.; Stork, D.; Wolff, G. Optimal brain surgeon and general network pruning. In Proceedings of the IEEE International Conference on Neural Networks, San Francisco, CA, USA, 28 March–1 April 1993; pp. 293–299.
42. LeCun, Y.; Denker, J.S.; Solla, S.; Howard, R.E.; Jackel, L.D. Optimal brain damage. In Proceedings of the Advances in Neural Information Processing Systems Conference, Denver, CO, USA, 27–30 November 1990; p. 2.
43. Molchanov, P.; Tyree, S.; Karras, T.; Aila, T.; Kautz, J. Pruning convolutional neural networks for resource efficient inference. *arXiv* **2017**, arXiv:1611.06440.
44. He, Y.; Liu, P.; Wang, Z.; Hu, Z.; Yang, Y. Filter pruning via geometric median for deep convolutional neural networks acceleration. *arXiv* **2019**, arXiv:1811.00250.